Data validation, interpolation and signal to noise increase in iterative PIV methods.

by

A. Lecuona, J. Nogueira and P. A. Rodríguez

Universidad Carlos III de Madrid
Department of Mechanical Engineering
c/ Butarque 15, 28911-Leganés, Madrid, Spain
E-Mail: lecuona@ing.uc3m.es

ABSTRACT

The scenario for data validation and interpolation algorithms in correlation PIV is changing. In the past, these algorithms were the last steps in the measurement chain. The iterative advanced correlation PIV methods have modified this. To implement them validation and interpolation between iterations are valuable steps. In this new context, the number of outliers that are acceptable is much larger than when no measurement is done after these steps. Moreover, in the advanced PIV measurements these algorithms have to process a spatial frequency content that is notably higher. This paper offers some insight on the behaviour of two usual statistical local validation operators *i. e.* local mean average and local median. In addition to that a new proposal for a statistical local validation operator is given. It corresponds to a refinement of a previous version presented by the authors in 1997. The refinement adapts the algorithm to the new scenario, showing interesting performance figures. The basis of the algorithm is to implement a local operator in which only authenticated vectors participate.

Concerning the field of data interpolation, some considerations are developed concerning the way to fill the holes in the velocity map when an outlier is detected. This includes comparisons between the use of interpolation and the use of secondary correlation peaks, as an alternative approach. Examples are given in which these peaks show large uncertainty. These situations are usually related with small wavelength displacements. In this frame, the ability of image distortion techniques to increase the signal to noise ratio and accuracy of the correlation peaks is studied.

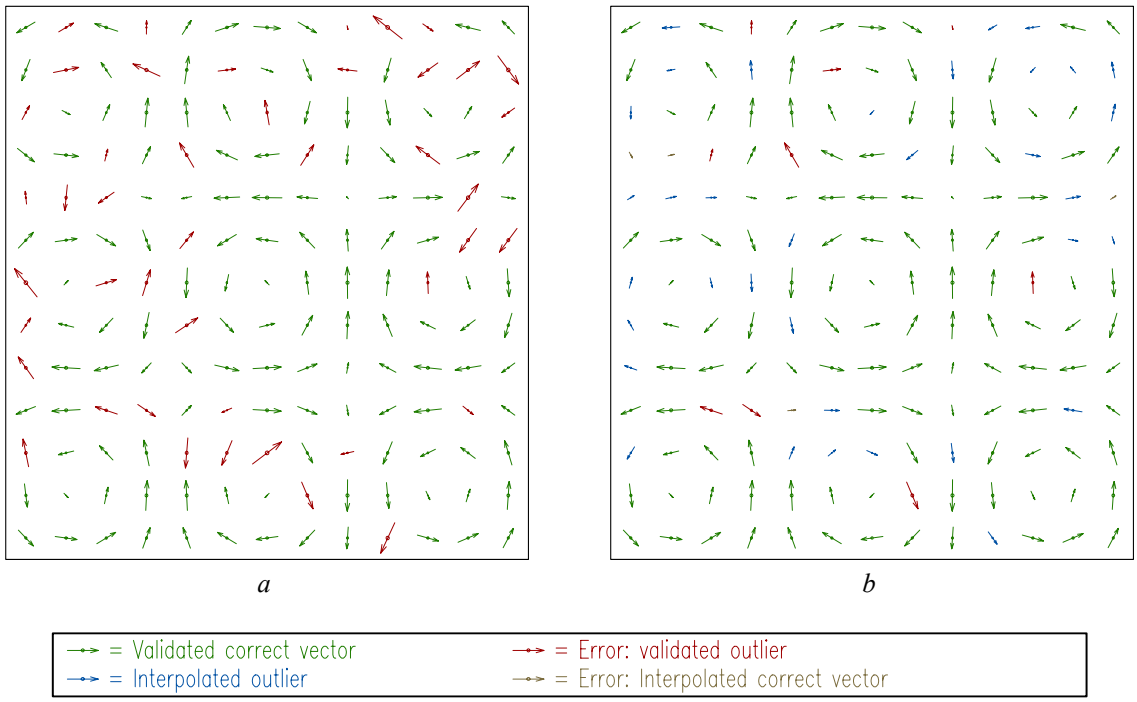

Fig. 1 Example of vector validation and interpolation with 25% of outliers and a small spatial wavelength, λ = 9.2 grid nodes. The scale for the vectors is arbitrary. a) Vector field containing outliers. b) Vector field after validation and interpolation. Validation has been implemented by means of a local authentication algorithm and interpolation by a 3 by 3 nodes iterative average. With this procedure the root mean square of the error, normalized with that of the signal, is reduced from rms(e)/rms(s) = 0.76 down to rms(e)/rms(s) = 0.28.

1. INTRODUCTION

The evolution of PIV methods has altered the requirements for data validation and interpolation algorithms. Initially, these algorithms were the last steps in the measurement chain. Vectors identified as outliers by validation algorithms were not measured again, and its substitution by a local interpolation or by secondary correlation peaks was objectable. Consequently, to obtain a representative measurement of a vector field, a low incidence of these outliers was mandatory. Acceptable presence of them was usually considered below 5% (Westerweel 1994, Nogueira *et al.* 1997a, among others). In addition to that, usually the vector fields analyzed were smooth to allow proper evaluation by conventional PIV systems. In these smooth vector fields with low incidence of outliers only the presence of discontinuity surfaces, like shock waves or unresolved shear layers, did introduce extra difficulty (Raffel *et al.* 1992). The validation and interpolation algorithms were generally designed for a high efficiency in this scenario. Furthermore, when filling the holes where the validation had identified outliers, it was not unusual to use second or third order interpolation algorithms to give a high degree of consistency with the rest of the measured vector field.

At the present time, this has changed due to the development of advanced PIV iterative methods (Huang *et al.* 1993, Soria 1996, Nogueira *et al.* 1999, Scarano and Riethmuller 2000, Fincham and Delerce 2000, Lecordier *et al.* 2001, Florio *et al.* 2002, Rohaly *et al.* 2002, among others). These methods use previous measurements to adapt or improve the processing in order to obtain better ones. In this measurement chain, the validation and interpolation steps are not the last steps, but usually a way to improve the quality of an initial or intermediate guess of displacements. Some of these advanced PIV methods have proved to give excellent results even in cases with large values of velocity dynamic range and strong velocity gradients (www.pivchallenge.org).

The first step in an advanced PIV algorithm is usually designed for robustness, this means being capable of not yielding too many outliers at the cost of a low spatial resolution. Nevertheless, its application to complex flowfields and set ups may result in a high occurrence of outliers (especially in locations with large vorticity values). In this situation, validation and interpolation algorithms can improve the displacement field guess in further iterations. This enhances the adaptation of the processing for another iterative measurement step. For these initial guesses the requirements in accuracy are less exigent than for final measurements. As a consequence, in iterative PIV algorithms, the old requirement for low number of outliers (<5%) is only relevant in the last iterations.

In addition to the large values of velocity dynamic range and gradients that they can face, the advanced PIV methods aim at obtaining high resolution (Hart 1999, Nogueira *et al.* 1999, Fincham and Delerce 2000, Scarano and Riethmuller 2000). Consequently, the velocity field can have far more content in small spatial wavelengths that it did with conventional systems.

In sections 1 and 2, this paper offers some insight on the behaviour of usual validation algorithms in this new scenario (*i. e.* small spatial wavelengths and large presence of outliers).

In these sections, the vectors identified as outliers are substituted by a local average of 3 by 3 nodes. This average is performed in an iterative way (Nogueira *et al.* 1997a) to include the circumstance of presence of several outliers in the same 3 by 3 neighbourhood. Nevertheless, a further insight in the way these vectors can be substituted is described in section 3. This includes comparison of interpolation versus use of secondary correlation peaks. It can be observed that in case of small wavelengths, in the order of few interrogation window sizes, the quality of the peaks is seriously affected. Section 4 presents some tests about the ability of image deformation algorithms to deal with this and enhance the signal to noise ratio in the correlation domain.

2. DATA VALIDATION

Along the development of data validation, several paths have given results of interest. The different operators can be classified in two kinds: (i) global operators which use the information of the whole flow field for the validation and (ii) local operators which use just the neighbours to a certain vector for its validation.

The former ones, even though they may seem coarse, can be quite helpful in preliminary steps. They can be used in a first pass before applying the second kind ones.

Among these global operators, the selection of a minimum and maximum threshold for a vector property (modulus, direction or a certain component) is very common. This can be done by an *a priory* knowledge of the flow characteristics or, in a more sophisticate way, by automatic decisions taken over the global histogram (Raffel *et al.* 1992).

For the local operators another sub-classification can be made: (*a*) operators based on fluid flow properties and (*b*) operators based on the local statistical likelihood.

Regarding the fluid flow properties, it is worth mentioning some operators based on the divergence or vorticity of the flow (Raffel *et al.* 1992, Fujita and Kaizu 1995, among others). These algorithms rely on a solid base, but as the PIV methods have evolved, the flows under analysis have grown in complexity. It is now usual to find sensible out of plane components. In 2D 2C or even 2D 3C measurements, the lack of a full 3D description of the flow reduces to some degree the strength of such systems. Consequently, the application of these algorithms is constrained by the type of fluid flow.

Due to its simple conception, operators based on statistical local likelihood are more common. This paper focuses on three of them:

- The local mean in a 3 by 3 nodes neighbourhood (Raffel *et al.* 1992)
- The local median in a 3 by 3 nodes neighbourhood (Westerweel 1994)
- A local authenticated vector operator (refined from the one in Nogueira *et al.* 1997a) that is described in section 2.1.

As any local operator, these three algorithms calculate a prediction of the expected value of a certain vector based on its neighbours. The difference between this prediction and the measured vector is called residual displacement (after Westerweel 1994). This residual displacement has to be evaluated to decide if the associated vector should be validated or not. The simplest evaluation can use a fixed threshold for the whole vector field. More complex options include local estimations of the flowfield variability. An example can be found in Raffel *et al.* (1992), where the differences between the moving average and the vectors that take part in its calculation define a local variability of the field, σ. This is used to implement an adaptive threshold in the form: C1+ σC2, where C1 and C2 are constants to be defined by the user. In this paper, the value of the threshold is studied for the three operators. This is performed in series of tests with different wavelengths. However, each wavelength is evaluated with a single threshold. The rationale behind this arbitrary decision is that, for small wavelengths and high content in outliers, the optimization of an adaptive threshold within each wavelength is a complex task beyond this study.

Before any evaluation of the different algorithms under study is done, some logical points can be drawn about them. The local mean performs a very good validation in presence of a few outliers and large spatial wavelengths, but as the number of outliers increases, the local prediction given by the neighbours (some of which may be outliers) becomes increasingly affected. The median gives a more coarse prediction in absence of noise. Nevertheless, it is less affected by neighbour outliers. Consequently, it gives better results than the mean, as the noise content increases. Actually, this is one of the most popular filters in image processing to reject "salt and pepper" noise, which is very similar to presence of outliers.

This line of thought leads to a further step. It would be ideal to apply an operator that only uses valid vectors. This is the idea behind the algorithm presented by Nogueira *et al.* (1997a). This algorithm locally evolves through the vector field trying to discriminate outliers. Thus the operator uses only what we call authenticated vectors, for its prediction of a displacement. The difficulty here rests in trying to reduce false authentications to the minimum. The objective of the algorithm designed in 1997 was only to overcome the problem of presence of discontinuities in smooth vector fields with few outliers. The change of scenario to small wavelengths and high number of outliers imposes a refinement in the algorithm that is further described in subsection 2.1.

2.1 Refinement of the local authentication algorithm.

Exhaustive test on this kind of algorithm in presence of small wavelengths and high percentage of outliers has lead to subtle but important refinements in reference to the version in Nogueira *et al.* (1997a). The result is a simpler version, which gives substantially better output. This refined algorithm is based on the following two considerations:

- The 1997's local operator calculated a high number of local predictions for each position, based on neighbours. This gives an excessively high probability of validating an outlier. In this version, the number of local predictions has been drastically reduced.
- The local mean and median in a 9 by 9 nodes neighbourhood have a first order or almost first order built-in character. To make predictions comparable to those, first order guesses are required. This point is further clarified below.

With these two considerations, the algorithm has been refined into the ensuing steps:

First step (identical to that in Nogueira *et al.* 1997a), is to identify a zone of local coherence. This is performed by calculating the following value for each grid node:

$$val = \frac{\sum_i |\vec{v}_i - \vec{v}_0|}{\sum_i |\vec{v}_i|} \qquad (1)$$

Where $|\ |$ is the vector module. In this expression $\vec{v}_i$ refers to the eight closest neighbor vectors to the grid node which velocity is $\vec{v}_0$ and to which *val* will be assigned. The location where this value reaches a minimum indicates a zone where vectors reach some degree of uniformity and therefore a neighborhood where vectors are coherent.

Second step is to evolve across the vector field identifying all the vectors coherent with the one found in the first step. This is done by checking all the neighbors that differ less than the chosen threshold from any of a set

of predictions. Here the set of predictions has been reduced in respect to those of the previous version. The maximum number of predictions then was 255 (only when all the surrounding vectors were authenticated). It is now reduced to a maximum of 5:

- One local average. Instead of checking the average of all the combination of *n* of the already validated vectors among the 8 neighbors that surround the one to be validated, only one average is checked. This average is that of all the vectors already validated among the 8 neighbors. As the number of validated vectors grows, this check is repeated in consecutive cycles. This may mean more and different checks on a single location; nevertheless, some of the checks with less number of vectors are avoided in respect to the previous version. This has been observed to improve the results in the case of high incidence of outliers and small spatial wavelengths.
- Four linear extrapolations. As already commented, at least a first order prediction is needed for results comparable to those of the mean and median. Here the 4 first order extrapolations depicted in figure 2 are checked with the vector to valalidate, if the associated vectors are validated. The reason for an extrapolation instead of an interpolation is that growing areas usually arrive to the vector to validate from one "side" instead of from the whole perimeter. In consequence, this extrapolation is needed to match the built-in character of first order prediction of the mean and almost first order of the median with 8 neighbours. Of course, occasionally it happens that the whole perimeter is used in the local average described in the previous point, but this will happen only after several "side" predictions have validated the neighbours. Extrapolation, when possible, provides these "side" predictions with the first order approximation requirement. Although extrapolation is more risky than interpolation, the tests in this paper show a good behaviour of this operator. An additional advantage is the predictable good performance on the edges of the vector field where the whole perimeter of the nodes is not available.

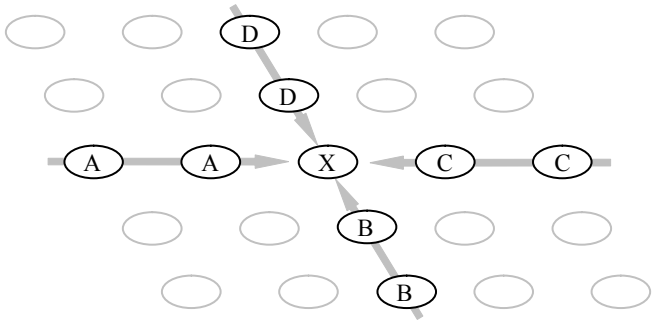

Fig. 2. Location of the 4 first order extrapolations in the validation of the vector in grid node X. The figure represents a 5 by 5 grid nodes neighbourhood. Each of the four couples marked with A, B, C and D respectively are the values to extrapolate a prediction on location X.

As new grid nodes are found to be coherent with the previous ones, the zone is expanded, and the check is repeated with all the neighbors to the authenticated vectors, *i. e.* those validated as coherent with the zone under study. When it does not add any new vector this step ends.

It can be argued that in this way, the mean and median operators are using only the 8 neighbours while this operator is using the 12 closest neighbours. To identify whether the improved performance of this algorithm was due to this fact, a test was done adding this prediction to the mean and median algorithms and no significant improvement was detected. In the rest of the paper usual 8 neighbours median and mean are used for clarity.

Third step is to repeat the first and the second steps on the remaining vectors. Each time that the third step is reached, the fully identified coherent regions in the second step are tagged. These tagged vectors are not used at all in the validation of subsequent regions. This is another difference in respect to the previous version, where these vectors were checked for coherence when evaluating other regions and, eventually, coherent regions were allowed to merge. This reduces the possibility of validating outliers.

After this step is fulfilled, several coherence domains are obtained. In a flow with discontinuity surfaces a coherence domain is expected to arise at each side. In a random vector region several domains containing a few vectors is what is expected.

Fourth step is to validate the domains with an appreciable number of vectors while the ones with a few are rejected. An estimation of the number of vectors that conforms a domain to validate is usually easy to set. The lower limit of such number corresponds to the maximum number of vectors that may constitute a coherent error. The upper limit would correspond to the minimum number of vectors that constitutes a flow field area behind a discontinuity. In general any number between these two limits is valid.

The order of magnitude of these limits can be sketched as follows. The maximum number of vectors that may be correlated within a coherent error is related to the size of the interrogation window of the PIV system. This is usually smaller than 64 by 64 pixels. On the other hand, the images are usually larger than 640 by 640 pixels. Consequently, the threshold can be set to 1% of the total number of vectors. Smaller features in the flow separated by discontinuities or larger window sizes are not usual, and should be treated with a special setup.

Usually this value can be changed up to 10% without noticeable difference, as it is not usual to try to depict such small zones behind a discontinuity. Although quite general, these cannot be universal recommendations as flow field configurations and PIV parameters can be very diverse. One example is the characterization of a lambda shock wave near a wall, where the lambda zone can be relatively small.

Any vector statistically non-coherent with its neighbours has to be eliminated with the proposed algorithm, unless they are many, grouped and coherent, something very unlikely. Anyway, an algorithm should check for this circumstance afterwards. The performance of this algorithm compared with those of the mean and median is tested in sections 2.2 and 2.3.

2.2 Performance of the local operators over velocity fields with no discontinuities.

A first evaluation and comparison of the performance of these algorithms has been performed over vector fields like the one depicted in figure 1. In these fields, combination of sinusoidal functions of a certain wavelength, λ, define vortical structures of half the wavelength in size. The particular displacements, s_x and s_y, follow expression (2):

$$\begin{aligned} s_x &= -A\cos(2\pi x/\lambda)\sin(2\pi y/\lambda) \\ s_y &= A\sin(2\pi x/\lambda)\cos(2\pi y/\lambda) \end{aligned} \qquad (2)$$

where the spatial coordinates x and y are measured in the same units than the wavelength. The amplitude, A, is arbitrary and will be use to normalize results.

Once the vector field is defined, a certain percentage of vectors are substituted by others with random values for each component within the same A to $-A$ limits. For simplicity, all these false vectors are named in the rest of the paper as outliers. Nevertheless, a small percentage of them may be coherent with the surrounding vectors just by chance.

The components of these outliers have been arbitrarily limited to the A to $-A$ range to depict a situation in which a global operator has already been implemented. In the ideal situation after such an implementation, all the vectors with larger component values have already been corrected. In consequence, local validation is needed for further refinement of the measured vector field.

Sets of tests were run for these conditions. Non-validated vectors were substituted using the iterative local average of 3 by 3 grid nodes commented in the introduction. In these tests, the root mean value of the error rms(e) has been normalized with that of the displacement vectors rms(s). To evaluate the performance of the different local validation algorithms, significant ranges of λ, percentage of outliers, and threshold values were covered. The information obtained in this way is depicted in several plots in the rest of this subsection.

A first important parameter is the minimum rms(e)/rms(s) obtained by each algorithm for each wavelength and content in outliers. This is plotted in figure 3.

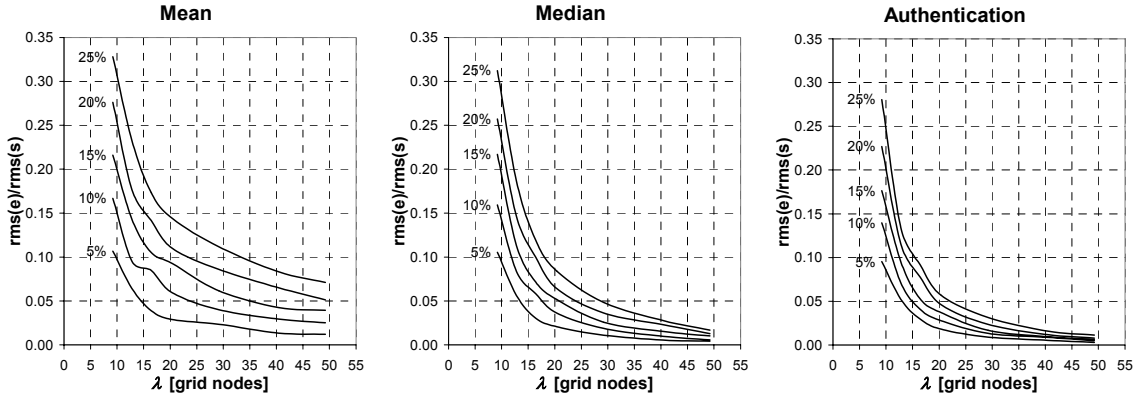

Fig. 3. Best possible performance of local operators as a function of wavelength and for several percentages of outliers content, operating over fields following expression (2).

These results correspond to different values of the threshold that evaluates the residual displacement at each percentage of outliers and wavelength. The optimum threshold value is smaller for larger wavelengths and smaller content in outliers. In all the cases, its variations with the wavelength were significant while that with the content in outliers was not. These variations ranged from 23% to 65% for the mean operator; from 11% to 66 % in the case of the median operator and from 4% to 37% in the case of the authentication operator. The rms(e)/rms(s) in

each field before the validation algorithms was applied is independent of the wavelength. Its value as a function of the percentage of outliers in these vector fields is presented in table 1.

Percentage of outliers	5%	10%	15%	20%	25%
rms(e)/rms(s)	0.33	0.47	0.57	0.66	0.75

Table 1. rms(e)/rms(s) as a function of the outliers content before validation, in the present paper.

In a real vector field, a large range of wavelengths would be simultaneously present. Consequently, the variation of the optimum threshold value with the wavelength is an important issue. To illustrate this, the variation of the rms(e)/rms(s) in the particular case of 25% of content in outliers is depicted in figure 4 as a function of the threshold value and the wavelength. The behaviour is qualitatively similar for the rest of tested wavelengths.

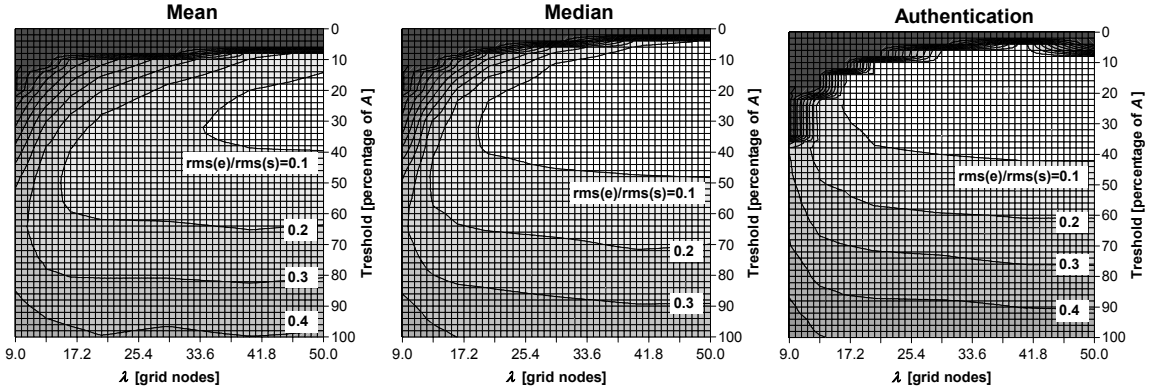

Fig. 4. Performance of local operators as a function of wavelength and the validation threshold at 25% content in outliers.

It can be observed that this variation is smaller for the case of the authentication operator. But this does not define a better behaviour, as it is apparent that the sensitivity to this parameter is also larger for this operator at all wavelengths. A test to evaluate whether the relation between these variations is favourable or not is to select a fixed threshold value for all cases. It is clear that the extreme situation corresponds to small wavelength and large content in outliers. Consequently, the optimum value of the threshold for each operator at small wavelength and large content of outliers has been chosen. These values are 66% of *A* for the mean, 65% of *A* for the median and 42% of *A* for the authentication algorithm. In this last case, due to the stepped change in performance at one side of the real minimum at 37% (see figure 4); a margin of 5% has been included. The results of this new test have been plotted in figure 5.

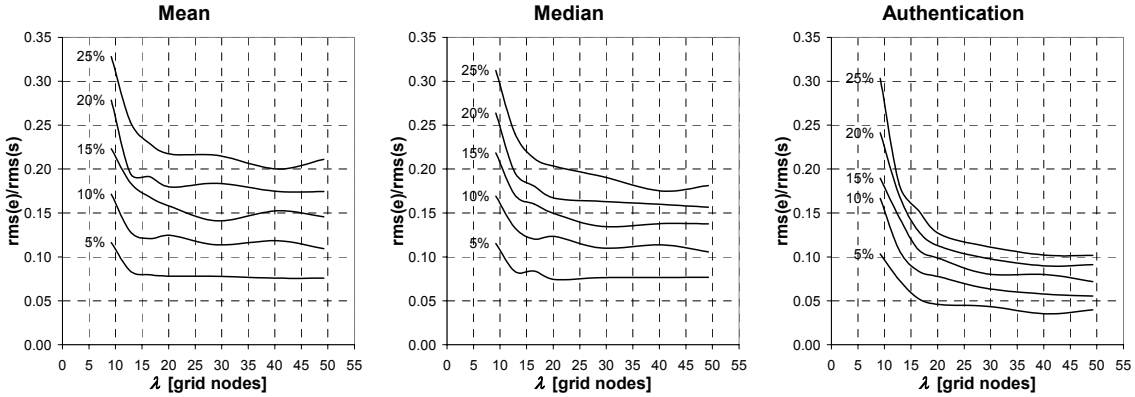

Fig. 5. Performance of local operators, as a function of wavelength and the percentage of content in outliers, for a fixed validation threshold. This threshold corresponds to almost the optimum at small wavelength (66% of A for the mean, 65% of A for the median and 42% of A for the authentication algorithm).

The authentication algorithm clearly shows better performance. Back to figure 4, it can be appreciated that this behaviour, better than that of the median, appears for a validation threshold value in the range from 37% up to 47%. This means a range of 10% where the authentication algorithm performs better than the median algorithm right at its best performance. The much-stepped growth of error of the authentication algorithm at low threshold values, even for small wavelengths, indicates that one must be careful on this. Although it could be considered a difficulty, it has also the advantage of indicating whether the selection of the threshold is correct or not.

As a conclusion of this subsection, authentication gives better results as expected, but at the cost of higher computing time and a more complex coding. Additionally, some care should be taken with the selection of the threshold, as the optimum performance rests close to a stepped worsening of performance for lower values of the threshold; although this last part may be used also as a key to automatize its selection. It should also be said that the increase of computing time is not relevant compared with the advanced PIV processing

This better performance is a side effect if we consider that the real reason to develop this algorithm is the presence of discontinuities in the vector field to validate. Next subsection studies in detail the differences of performance in presence of a discontinuity in the flow field.

2.3 Performance of the local operators over velocity fields with discontinuities.

It is not unusual to observe PIV applications where a shock wave or an undersampled shear layer produces a discontinuity in the vector field. As the PIV methods grow in capabilities, these situations are more common. Validation in these situations introduces an extra difficulty. It can be expected that mean or median filters that do not discriminate vectors belonging to one or other side of a discontinuity would have a difficult task when validating in the discontinuity. The authentication operator, on the other hand, is expected to have a smaller increase of difficulties. To check this idea, a velocity step function has been added to the field used in the previous subsection. *i. e.* a vertical velocity of value *A* has been added to the left half of the flowfield, while a vertical velocity of value *A* has been subtracted to the right half. A detail of the resulting vector field is depicted in figure 6 for illustration.

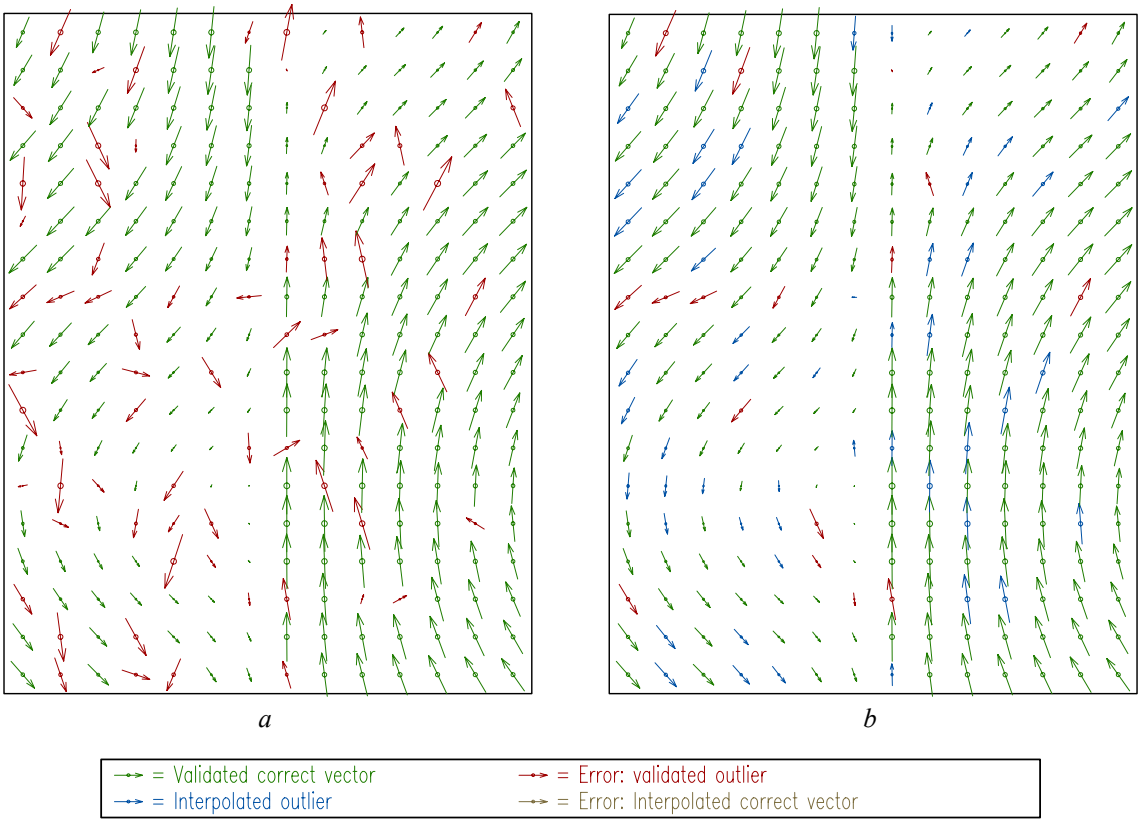

Fig. 6 Example of vector validation and interpolation with 25% of outliers and a discontinuity in the flow field (λ = 29.2 grid nodes). The scale for the vectors is arbitrary. a) Vector field containing ouliers. b) Vector field after validation and interpolation. Validation has been implemented by means of a local authentication algorithm and interpolation by a 3 by 3 nodes iterative average.

For this case, the rms(s) has been calculated in respect to the mean value for each half. This gives the same magnitude than in the case of section 2.2, obviating the step function. This is coherent with the usual interest on the variations of the flowfield at both sides. In this subsection, the value of the rms(e)/rms(s) only includes the two columns of vectors at both sides of the discontinuity. This is so because the behaviour in the rest of the vector field is similar to that already described in the previous subsection. For these localized, but interesting zones, the analysis of the previous subsection was repeated. Similarly to figure 3, the minimum rms(e)/rms(s) obtainable when varying the threshold value, for each wavelength and contents in outliers, is depicted in figure 7.

Like in the previous subsection, the optimum threshold value for each case is generally smaller for larger wavelengths and smaller contents in outliers. The variations of this value ranged from 110% to 155% for the mean operator; from 95% to 150% in the case of the median operator and from 25% to 85% in the case of the

authentication operator. Nevertheless, differently to the previous subsection, the variation of the rms(e)/rms(s) as a function of the threshold value was small near this minimum in every case.

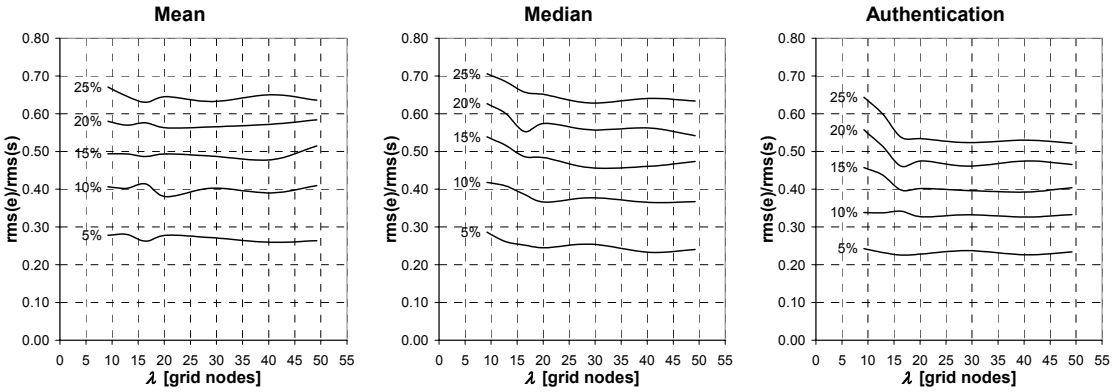

Fig. 7. Best possible performance of local operators as a function of wavelength and percentage of outliers content at both sides of a discontinuity of amplitude 2A, in fields following expression (2).

The problem arises when it is taken into account that these values for the threshold are very different to those used to validate the rest of the flowfield, especially for the mean and median algorithms. Consequently, a test similar to that in figure 5 has been run. The value of the threshold was fixed to the same values than in the previous subsection (66% of A for the mean, 65% of A for the median and 42% of A for the authentication algorithm). These values allow finding out the behaviour of the operators when they arrive to a discontinuity from validating each side of the flowfield. The results are plotted in figure 8. A local adaptation of the threshold is always possible but a good behaviour without it implies fewer problems when developing such adaptive routine.

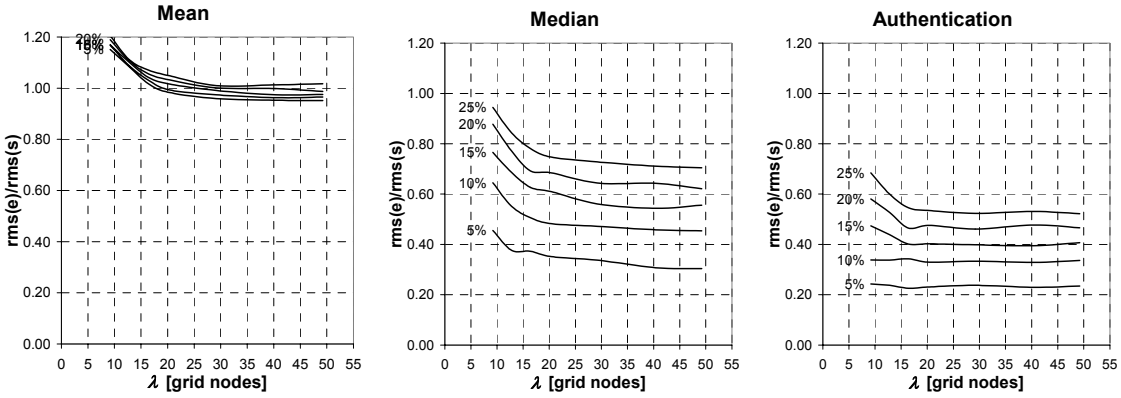

Fig. 8. Performance of local operators, as a function of wavelength and for several percentages of content in outliers, for a fixed validation threshold (66% of A for the mean, 65% of A for the median and 42% of A for the authentication algorithm) at both sides of a discontinuity of amplitude 2A, in fields following expression (2). This threshold corresponds almost to the optimum at small wavelengths in figures 3 and 4.

The conclusion of this section is that the local authentication algorithm shows interesting performances. Nevertheless, a certainly more complex coding than the mean and median operators is behind its simple concepts. More research is still needed to ascertain comparison with local median and mean multipass iterative schemes and in presence of different kinds of discontinuities within the flow field.

3. INTERPOLATION AND MULTIPLE PEAK EVALUATIONS.

To substitute the outliers detected by the validation algorithm, the two usual options are: (a) to interpolate a value using the neighbours or (b) to use secondary peaks from the correlation plane. It seems clear that interpolation in a situation where a large number of outliers arise cannot be accurate, but in this scenario, it is also possible that the distortion on secondary peaks gives also a peak location error. To establish a comparison on performance of both techniques, a particular case related to the fields already used for validation is tested here. It is not an exhaustive research but can throw some light in the subject.

For this task, a couple of synthetic image was generated. They contain no noise except for the discretization of the 8 bits square pixels. In these images, all the particles have gaussian shape with the same brightness (grey level of 100 out of the 255 possible) and size (e^{-2} diameter, d = 2pixels). The mean distance between particles is $\delta = 2$ pixels. The grey level was added on those particles overlapping. In this situation, it is expected that only the

displacement field would distort the location of the correlation peaks. The evaluation methods can introduce some peak locking (Nogueira *et al.* 2001a), but it is not built in the images as the diameter of the particles is large enough (Westerweel 1998).

The chosen displacement field was that of the expression (2) with a wavelength, λ = 16.4 grid nodes and an amplitude of A = 4.5 pixels. The selected grid spacing was Δ = 4 pixels (*i. e.* λ = 65.6 pixels). The size of the interrogation window used was F = 16 pixels.

In this situation the first and second highest correlation peaks at the central 9 by 9 pixels zone in the correlation plane were chosen. Consequently, a scenario like the one depicted for validation in section 2.2 results, where no component can be larger than 4.5 pixels. The presence of outliers was considered when the second peak was closer to the real displacement than the first. Further peaks were not considered for clarity. This gives a figure of 16% of outliers.

The outliers in the displacement measurements were corrected in two different ways: (i) by using the second correlation peak. (ii) by means of an iterative 3 by 3 pixels moving average. A portion of this image is given in figure 9.

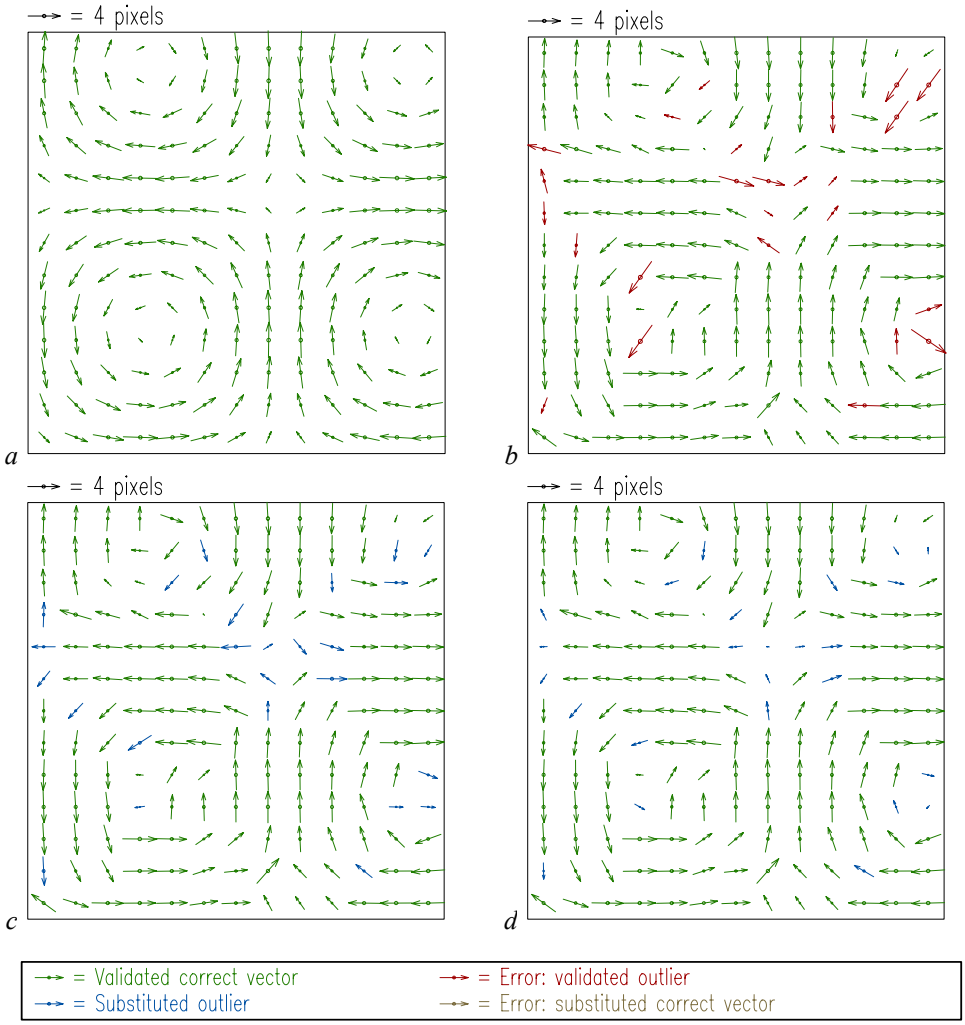

Fig. 9 Example of different outlier substitution methods. a) Original displacement field Δ = 4 pixels. b) Measured vector field containing ouliers F = 16 pixels. c) Substitution of outliers by second correlation peak. d) Substitution of outliers by 3 by 3 iterative moving average. Some comments concerning the squareness of the measured vortical structures are given below in the text.

Owing to the small wavelength and the large gradients the error in the measurement, considering always the main peaks, was rms(e)/rms(s) = 0.57. The one obtained supposing a perfect validation algorithm and substituting all the outliers by the second correlation peak is rms(e)/rms(s)= 0.42. In this particular case, the alternative solution of iterative 3 by 3 local average gives a figure of rms(e)/rms(s)= 0.36.

It can be observed that the distortion of the position of the PIV correlation peaks can be severe in situations where a high resolution is needed. It can also be observed that not only at outlier positions, but also the first peak, can be seriously distorted. Consequently, it seems like interpolation of higher than first order in intermediate steps of an advanced algorithm would not represent necessarily an improvement. In conclusion, the use of secondary

correlation peaks or high order interpolation schemes in complex flowfields is as objectable as a simple first order interpolation.

The squareness present in figure 9 measurements is a feature that may appear in a single pass PIV systems (Nogueira *et al.* 2002). It is not related to peak locking but to the displacement fields themselves (it can be observed that in this case the rms(e) in the initial measurement corresponds to 1,8 pixels, far from subpixel errors). It appears when the wavelength is less than a few interrogation window sizes, especially close to twice the size of the window. It is more apparent with high interrogation window overlapping and high seeding density of small monodisperse particles. It can be reduced by the use of weighting functions on the interrogation window or lowpass filters in the output. In these cases, care should be taken to reduce the spurious high frequencies raised by the squareness without loosing too original much signal. Iterative advanced algorithms are especially sensitive to these choices but, correctly set, they can give accurate results. This can be appreciated in figure 10a. In this figure the analysis of the previous PIV couple of images has been performed by means of LFC-PIV (Nogueira *et al.* 2001b). The result gives a figure of ms(e)/rms(s)= 0.11 with F = 64 pixels. This indicates that the results in figure 9b are not produced by errors in the definition of the PIV images; the distorted position of the correlation peak is given by the velocity field. Also a conventional single pass PIV with F = 16 pixels has been applied over an image with a displacement field of larger wavelength λ = 131,2 pixels (this implies a "vortex" of 65.6 by 65.6 pixels). The output is presented in figure 10b. It gives an rms(e)/rms(s)= 0.14, showing that the conventional PIV algorithm is performing correctly for large wavelengths.

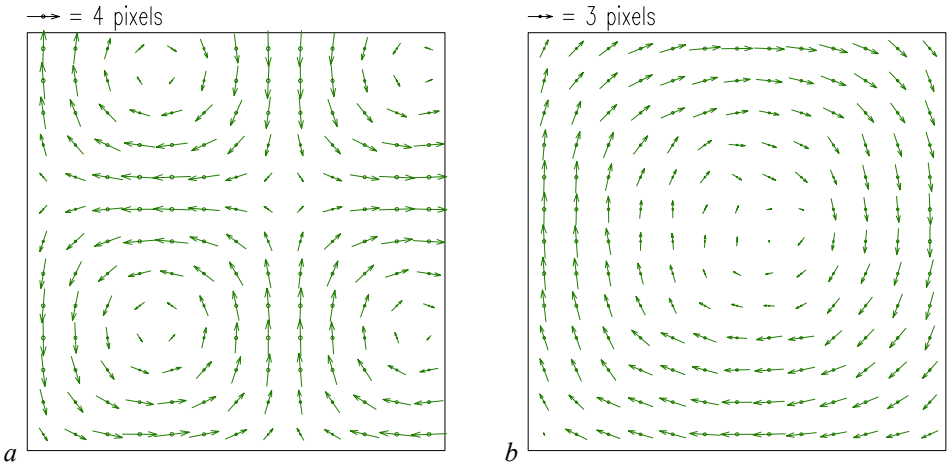

Fig. 10 Performance related to the comments on the squareness of the vortical structures in figure 9. a) LFC-PIV, F = 64 pixels, measurement of the images corresponding to a displacement field of expression (2) with λ = 65.6 pixels. b) Single pass conventional PIV, F = 16 pixels, measurement of images corresponding to a displacement field of expression (2) with λ = 131.2 pixels.

The example here depicted about the distortion on the location of the correlation peaks is just an example. To give a more complete picture it would be useful to study situations where only a large gradient is present (like a single vortex). Also the situation with a discontinuity in the flow field can be of interest. At both sides of a discontinuity the interpolation operator would arrive to a complex situation while the secondary peaks could have added little difficulty to a normal situation.

4. ENHANCEMENT BY MEANS OF IMAGE DEFORMATION.

The measurement in a PIV system is mainly based in the identification of a peak in the correlation. About this identification, two points are important in the performance of the PIV system:

- The noise level. Under many circumstances, secondary peaks can become even larger than the correct one. Some sources of these spurious peaks are the noise in the PIV images, the displacement gradients within the interrogation window and the presence of spurious correlation between first and second images of different particles in the PIV frames to correlate.
- The location of the peak itself. As commented in the previous section and in Nogueira *et al.* (2002), the displacement gradients within the interrogation window can produce main peaks which correspond to a real displacement but not to the one searched (*i. e.* the one that corresponds to the center of the interrogation window).

The iterativeness of the advanced PIV methods was initially designed to achieve a signal to noise enhancement. This is focused mainly in reducing problems related to the first point. But, as the noise characteristics are generally unknown and the spurious correlation of particles cannot be avoided in correlation, the focus is to increase the

signal peak instead of reducing these noise sources. The first approach was the shifting of the interrogation windows. This increases the signal to noise ratio by reducing the in-plane loss of particles between correlating windows. More recently, image deformation algorithms have aimed at reducing also the displacement gradients within the interrogation window. This gives very valuable improvements when dealing with features with small wavelengths. A comparison of signal to noise enhancement has been performed in the particular case of the previous subsection (λ = 65.6 pixels). The local signal to noise (S/N) ratio from Nogueira et al (2001b) has been used:

$$S/N = \frac{Signal\ peak - Average\ value}{Highest\ noise\ peak - Average\ value} \qquad (3)$$

In this expression the average value is obtained in the correlation domain averaging all the values smaller than the smallest of both peaks defined. The peak closest to the real displacement, out of the two main ones, has been arbitrarily defined as signal peak. Three situations are analyzed for 16 by 16 pixels windows: (a) No shift between windows. (b) Discrete shift of windows. (c) Compensation of the particle pattern deformation by image distortion. The results are plotted in figure 11.

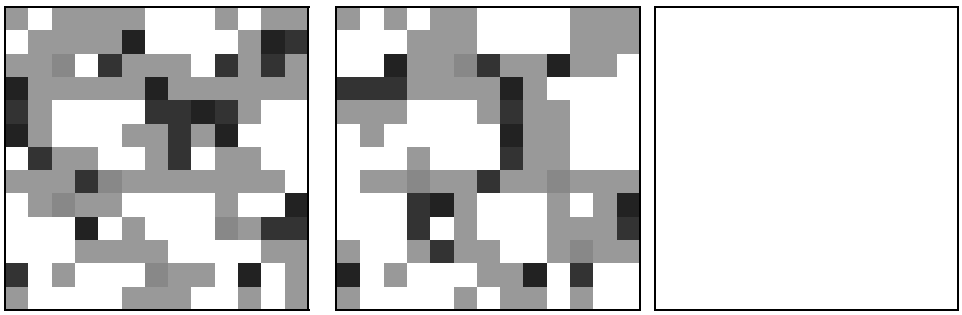

Fig. 11. Analysis of the signal to noise ratio in a couple of PIV images corresponding to the displacement field in fig. 9a. s/n ratio code for the different grid nodes: >2 - White; 2 to 1 - Grey; <1 - Black. (a) No shift of interrogation windows. (b) Only discrete shift of interrogation windows. (c) After Compensation of the particle pattern deformation.

In this figure, the places with $s/n < 1$ mean that the second peak is closer to the real displacement than the first peak. The outstanding performance of case c) is to be expected as the synthetic images contained negligible noise. It is relevant to observe that for small wavelengths, the improvement in case b) respect to case a) is modest.

The second issue in this subsection, *i. e.* the location of the correlation peak, is closely related to the previous one. Nevertheless, it corresponds to a different concept. It comes from correct correlation of images of the same particle in the couple of PIV images. The problem here is that due to the displacement gradients within the interrogation window, a displacement different to that in the center of the window is obtained as main peak giving the poor result presented in figure 9b. The shift of the interrogation windows does not clearly improve these results. Therefore, to correct this behaviour some other techniques have to be used. Weighting the interrogation window can improve results (Nogueira *et al.* 2001b), but a much more effective way is again the compensation of the particle pattern deformation by means of image deformation.

About the way this compensation is performed, two different approaches depicted in figure 12 are offered:

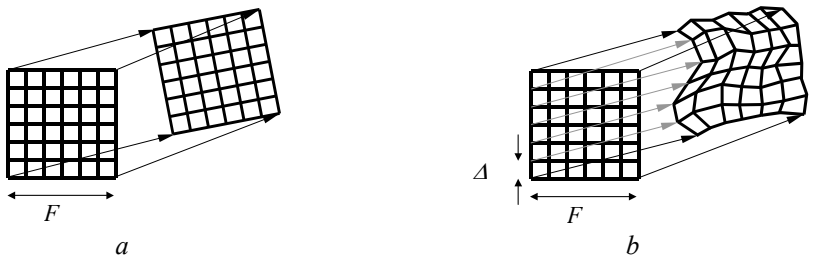

Fig. 12. Two extreme ways in the implementation of the compensation of the particle pattern deformation. (a) Distortion using only the grid nodes of the window corners, (b) using all the grid nodes at high overlapping. Only some displacement vectors are plotted in the second way for clarity.

(*a*) The deformation of the interrogation window based on its size F: only the displacements at the corners are used (a more complete version would use up to 9 grid nodes at 50% of overlapping). In this way the possible instabilities coming from image distortion iteration are avoided (Nogueira *et al.* 2002), but the correction of gradients is limited by the use of few points.

(*b*). Based on the grid distance, Δ, with high overlapping: in this case, special care has to be taken about instabilities and to control the frequency response of the PIV that allows for description of wavelengths smaller than the interrogation window (Nogueira 1997b, Nogueira *et al.* 1999 and 2001b). On the other hand, the compensation of the particle pattern deformation is less limited. With this technique, results like the one presented at figure 10a can be obtained for even much smaller wavelengths (Nogueira *et al.* 2001b).

As a conclusion of this section, it seems that image distortion is a good way of dealing with small wavelength features. This explains why its first implementations focused on dealing with large gradients (Huang *et al.* 1993, Jambunathan *et al.* 1995, among others) have been recuperated in the actual advanced PIV methods to deal with small wavelengths (Nogueira 1997b, Nogueira *et al.* 1999 and 2001b, Scarano and Riethmuller 2000, Fincham and Delerce 2000, among others).

6 CONCLUSIONS

The scenario for the application of data validation and interpolation has evolved recently. Now, the processing of vector fields with a large content in outliers and presence of small wavelength features is important for intermediate steps of advanced PIV methods.

Within this frame, a refined version of a validation algorithm presented by the authors in 1997 has been proposed in this paper. The performances of this algorithm confirm that evolving through the vector field authenticating the vectors to be used by a local validation operator is an interesting strategy.

The algorithm proposed following this philosophy presents better performances than the usual mean and median operators, especially in presence of discontinuities in the flow according to the tests performed.

The counterpart is a certainly more complex coding.

Once the validation has been performed, the identified outliers have to be substituted. About vector substitution, in the above-mentioned scenario, some ideas have to be taken into account. Performance in particular cases show that a first order interpolation, using the neighbours to the vector to substitute, can be a better option than using the secondary correlation peak for the substitution.

Furthermore, it is easy that the first peak location is so much deviated that interpolations of higher than first order would not mean an advantage.

Finally, section 4 indicates that in order to obtain an acceptable measurement in presence of these peak location errors, window shift is not enough; it requires image deformation. In consequence, image deformation does not only increase the signal to noise ratio, but also removes peak location errors coming from the PIV non-linearity.

ACKNOWLEDGEMENTS

This work has been partially funded by the Spanish Research Agency grant AMB1999-0211, DPI2000-1839-CE, Feder 1FD97-1256 in collaboration with the Universidad de Las Palmas de Gran Canaria and under the EUROPIV 2 project (A JOINT PROGRAM TO IMPROVE PIV PERFORMANCE FOR INDUSTRY AND RESEARCH) is a collaboration between LML URA CNRS 1441, DASSAULT AVIATION, DASA, ITAP, CIRA, DLR, ISL, NLR, ONERA, DNW and the universities of Delft, Madrid (Carlos III), Oldenburg, Rome, Rouen (CORIA URA CNRS 230), St Etienne (TSI URA CNRS 842), Zaragoza. The project is managed by LML URA CNRS 1441 and is funded by the CEC under the IMT initiative (CONTRACT N°: GRD1-1999-10835)
(¿DGICYT TAP96-1808-CE, PB95-0150-CO2-02?)

REFERENCES.

Di Florio D Di Felice F Romano GP 2002. “Windowing, re-shaping and re-orientation interrogation windows in particle image velocimetry for the investigation of shear flows” Meas. Sci. Technol. 13: 953–962

Fincham A M and Delerce G 2000 “Advanced optimisation of correlation imaging velocimetry algorithms” Exp. Fluids 29/7 S13–22

Fujita I and Kaizu T 1995 "Correction method of erroneous vectors in PIV" Journal of Flow Visualization and Image Processing, vol. 2, pp. 173-185.

Hart DP 1999 “Super-Resolution PIV by Recursive Local-Correlation”. Journal of Visualization. Vol: 3 num: 2.

Huang H T Fiedler H E and Wang J J 1993 "Limitation and Improvement of PIV (Part II: Particle image distortion, a novel technique)" Experiments in Fluids, vol. 15, pp 263-273.

Jambunathan K, Ju X Y; Dobbins B N and Ashforth-Frost S 1995 “An improved cross correlation technique for particle image velocimetry”. Meas. Sci. Technol. 6: 507-514.

Lecordier B Demare D Vervisch LMJ Réveillon J Trinité M 2001 “Estimation of the accuracy of PIV treatments for turbulent flow studies by direct numerical simulation of multi-phase flow” Meas. Sci. Technol. 12 (2001) 1382–1391

Nogueira J Lecuona A and Rodríguez P 1997a "On the design of some PIV postprocessing filters" 7th International Conference Laser Anemometry Advances and Applications. University of Karlsruhe, Germany, September 8-11.

Nogueira J 1997b “Contribuciones a la técnica de velocimetría por imagen de partículas (PIV)” PhD Thesis ETSIAeronáuticos, Universidad Politécnica de Madrid, Spain

Nogueira J, Lecuona A and Rodríguez PA (1999) “Local Field Correction PIV: On the increase of accuracy of digital PIV systems”. Exp. Fluids 27/2: 107-116.

Nogueira J; Lecuona A; Rodríguez P A 2001a “Identification of a new source of peak-locking, analysis and its removal in conventional and Super-Resolution PIV techniques”. Exp. Fluids 30/3: 309-316.

Nogueira J, Lecuona A and Rodríguez P A (2001b) Local field correction PIV, implemented by means of simple algorithms, and multigrid versions. Meas. Sci. Technol. 12: 1911-1921.

Nogueira J, Lecuona A Ruiz-Rivas and Rodríguez P A (2002) “Analysis and alternatives in two-dimensional multigrid particle image velocimetry methods: application of a dedicated weighting function and symmetric direct correlation”. Meas. Sci. Technol. 13: 963-974.

Raffel M Leitl B and J Kompenhans 1992. "Data validation for particle image velocimetry" 6th Int. Symp. on Appl. of Laser Techniques to Fluid Mechanics, Lisbon, Portugal, July 20-23.

Rohály J Frigerio F Hart DP 2002 “Reverse hierarchical PIV processing” Meas. Sci. Technol. 13: 984–996

Soria J 1996 “An Investigation of the Near Wake of a Circular Cylinder Using a Video-Based Digital Cross-Correlation Particle Image Velocimetry Technique”. Experimental Thermal and Fluid Science. 12: 221-233.

Scarano F and Riethmuller M L 2000 “Advances in iterative multigrid PIV image processing”. Exp. Fluids 29 S051–60

Westerweel J 1994. "Efficient detection of spurious vectors in particle image velocimetry data" Experiments in Fluids 16, Springer-Verlag, pp. 236-247.

Westerweel J 1998 “Effect of sensor geometry on the performance of PIV”. 9th Int. Symp. on Applications of Laser Techniques to Fluid Mechanics. Instituto Superior Técnico, Lisbon, Portugal.